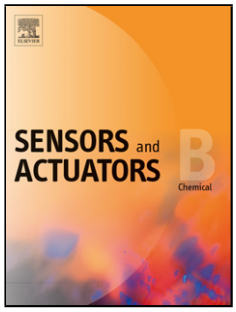

Title: Development of an improved ligand mimetic calibration system for the analysis of iron(III) in seawater using the iron(III) chalcogenide glass ion selective electrode: A combined mechanistic and analytical study

Author: Mark Maric Manzar Sohail Jean-Pierre Veder Roland De Marco

PII: S0925-4005(14)01072-7
DOI: http://dx.doi.org/doi:10.1016/j.snb.2014.09.003
Reference: SNB 17379

To appear in: *Sensors and Actuators B*

Received date: 7-5-2014
Revised date: 9-8-2014
Accepted date: 1-9-2014

Please cite this article as: M. Maric, M. Sohail, J.-P. Veder, R. De Marco, Development of an improved ligand mimetic calibration system for the analysis of iron(III) in seawater using the iron(III) chalcogenide glass ion selective electrode: A combined mechanistic and analytical study, *Sensors and Actuators B: Chemical* (2014), http://dx.doi.org/10.1016/j.snb.2014.09.003

Development of an improved ligand mimetic calibration system for the analysis of iron(III) in seawater using the iron(III) chalcogenide glass ion selective electrode: A combined mechanistic and analytical study

Mark Maric[a], Manzar Sohail[b,c], Jean-Pierre Veder[d], Roland De Marco[b,a*]

[a]Nanochemistry Research Institute, Department of Chemistry, Curtin University, GPO Box U1987, Perth, Western Australia 6845, Australia

[b]Faculty of Science, Health, Education and Engineering, University of the Sunshine Coast, Locked Bag 4, Maroochydore DC, Queensland 4558, Australia

[c]Current Address: Centre of Research Excellence in Nanotechnology, King Fahd University of Petroleum and Minerals, Dhahran 31261, Saudi Arabia

[d]CSIRO Mineral Resources Flagship, Box 312, Clayton South, Victoria 3169, Australia

* Corresponding author: Tel.: +61 7 5430 2867; Facsimile: +61 7 5456 5544; E-mail: rdemarc1@usc.edu.au

Abstract

Further to previous work on a seawater ligand mimetic calibration system for the electroanalysis of iron(III) in seawater using the iron chalcogenide glass ion-selective electrode (ISE), this study utilized alternative blends of synthetic ligands, in order to fine-tune and optimize the calibration response characteristics of this sensor for the electroanalysis of free iron (III) in seawater. Herein, an alternative calibration system (ACS) was derived using a mixture of 10^{-4} M iron(III) chloride, 10^{-4} M ethylenediaminetetraacetic acid (EDTA), 10^{-3} M copper(II) sulfate, 5 x 10^{-3} M ethylenediamine (EN) and 0.60 M sodium chloride yielding a Nernstian response of about 30 mV decade^{-1}. The electroanalysis of free iron(III) in seawater using the ACS generated a free iron(III) level commensurate with the predicted organic and inorganic speciation of iron(III) in seawater. Furthermore, electrochemical impedance spectroscopy (EIS), synchrotron radiation X-ray photoelectron spectroscopy (SR-XPS) and near edge X-ray absorption fine structure (NEXAFS) spectroscopy have demonstrated that the surface reaction processes of this membrane in the ACS are comparable to those experienced in a natural seawater matrix. Ultimately, this study demonstrated that the ACS can mimic the surface chemistry and concomitant potentiometric response characteristics of the iron(III) sensor in seawater, enabling reliable electroanalyses of free iron(III) in seawater.

Keywords: Iron chalcogenide glass; iron(III) sensor; seawater ligand mimetic system; modified surface layer; XPS; NEXAFS.

1. Introduction

Although iron is the fourth most abundant element in the earth's crust, it is only present in trace amounts (i.e., 0.02 to 1 nM) in the open ocean [1]. Iron is an extremely important bioactive trace metal in the ocean, as it limits phytoplankton production and is also pivotal in regulating carbon dioxide concentrations in the atmosphere [2]. The following notion was exemplified by an iron fertilization experiment, which demonstrated that the addition of iron to high nutrient/low chlorophyll areas of the ocean stimulated the growth of phytoplankton and other related ancient microorganisms [2-4]. Due to the ecological implications associated with iron in seawater, a robust and accurate method for the monitoring of iron(III) in seawater is of considerable interest to marine scientists and oceanographers.

While there is an array of *ex situ* techniques that can be employed in the determination of iron(III) in seawater (i.e. cathodic stripping voltammetry, chemiluminescence, etc.), these methods are susceptible to experimental uncertainties [5, 6]. These experimental errors arise mainly due to changes in the speciation of the metal, when a sample is taken from its natural environment [5, 7]. Ion-selective electrodes (ISEs) can overcome these disadvantages since they are capable of monitoring *in situ* metal ion concentrations [6-9]. Furthermore, a significant advantage of ISEs over other *ex situ* techniques is that, while *ex situ* methods are proficient at determining the total metal concentration, they often cannot provide information about the levels of free metals in solution [5, 7, 8]. On the other hand, ISEs are capable of sensing the free ion activity, which is widely regarded as a master variable governing the uptake and toxicity of metals by marine micro-organisms, subsequently providing an analytical technique capable of monitoring the fate and impact of trace metals in the environment [6-9].

Potentiometric sensors derived from chalcogenide membranes have attracted considerable interest for the analysis of various metals [10]. Early studies undertaken in Vlasov's laboratory [11, 12] established that chalcogenide glass ISEs can be employed in

environmental monitoring. Chalcogenide glasses are materials that comprise any one of the chalcogen elements, which are located in Group 6 of the periodic table (i.e. sulfur, selenium etc.). One of the most widely used Fe(III) ISEs is based on a chalcogenide glass membrane [$Fe_{2.5}(Se_{60}Ge_{28}Sb_{12})_{97.5}$] [12]. Early work by Vlasov, Bychkov and Legin [13] demonstrated that the detection limit of the Fe(III) chalcogenide glass ISE in unbuffered iron(III) solutions is pFe ~ 5.7. Recent studies by De Marco and Mackey [14] have shown that the Fe(III) ISE can be calibrated down to pFe ~ 23 in citrate and salicylate iron(III) buffers. Further research has shown that careful preparation of the electrode, combined with a hydrodynamic flow regime (i.e. continuous flow analysis), minimizes membrane fouling and enables trace analyses of metals in seawater [15]. De Marco et al. [16] used continuous flow analysis (CFA) ISE potentiometry in the rapid and reliable determination of free Fe(III) in organic free, UV photo-oxidized seawater. In a review by De Marco, Clarke and Pejcic [10], it was suggested that the use of synthetic ligands in an iron(III) calibration standard could mimic the iron(III) complexation capacity and electrode surface chemistry of the iron(III) chalcogenide glass ISE in natural seawater. Significantly, De Marco et al. [17] observed that, in artificial seawater, the surface crystalline phases of the sensor were vigorously attacked by chloride and hydroxide ions, but this deleterious ligand effect was not observed when the electrode was exposed to natural seawater. Subsequently, De Marco et al. [17] postulated that the natural organic ligands of seawater (i.e., humic and fulvic acids) are influencing the reaction chemistry of the electrode in a disparate fashion to that experienced in an artificial calibration system [17]. Consequently, De Marco and Martizano [18] developed a seawater ligand mimetic system, comprising a blend of different synthetic ligands in an attempt to simulate the influence of natural organic ligands in seawater. Further research conducted by De Marco and Martizano [18] demonstrated that the seawater ligand mimetic system yielded a Nernstian linear response using CFA ISE potentiometry. Despite these positive outcomes, De Marco et al. [17] established that the seawater ligand mimetic system is imperfect, as evident by results obtained using electrochemical impedance spectroscopy/synchrotron radiation-grazing incidence X-ray diffraction (EIS/SR-GIXRD) where non-identical surface chemistry effects were noted in natural seawater and the seawater ligand mimetic system,

demonstrating that there is scope for optimization and improvement of this iron(III) sensor calibration system.

The principal objective of this study was to develop a new and improved calibration system, which will yield superior electrochemical behaviour, thereby affording more reliable electroanalyses of free iron(III) in seawater. Accordingly, we have explored several synthetic ligands, with a view of fine-tuning and optimizing the calibration response characteristics of the iron(III) sensor. As a key to this investigation, it has been necessary to investigate the mechanistic chemistry of the chalcogenide glass iron(III) ISE and the concomitant influence of seawater and the new seawater ligand mimetic calibration system on the response characteristics of the iron(III) ISE. In this context, the authors have employed a state-of-the-art electrochemical surface analysis scheme employing EIS, synchrotron radiation-X-ray photoelectron spectroscopy (SR-XPS), near edge X-ray absorption fine structure (NEXAFS) and CFA potentiometry in an evaluation of the sensor response characteristics, so as to enable the development of an improved calibration system. Finally, the reliability of this improved seawater ligand mimetic calibration system was verified through the electroanalysis of free iron(III) in natural seawater.

2. Materials and Methods

2.1. Iron(III) Chalcogenide Glass Electrode

The chalcogenide glass membrane Fe(III) ISE and rotating disk electrode (RDE) with a composition of $[Fe_{2.5}(Se_{60}Ge_{28}Sb_{12})_{97.5}]$, was previously prepared by the De Marco Research Group, according to the procedure described by Koenig and Grabner [19]. In order to undertake meaningful surface and electrochemical studies of the Fe(III) chalcogenide ISE, it was necessary to clean the membrane surface prior to analysis. This was accomplished by using Struers silicon carbide paper of various grit sizes (viz. P500, P1000, P2400 and P4000). Membranes were polished for approximately 2 minutes with each grade of silicon carbide paper that had been wetted with Milli-Q water. The membranes were subsequently polished

extensively in a methodical stepwise approach by utilizing diamond spray of decreasing sizes (3 micron, 1 micron and 0.1 micron). The polishing pad and diamond sprays were both obtained from Kemet. The polished surface was rinsed with copious amounts of Milli-Q water and ethanol, and blotted dry on a tissue.

2.2. Reagents

Analytical grade reagents were employed in all cases, and all solutions were prepared using ultra high purity Milli-Q water (0.055 μS cm^{-1}). Solutions were prepared by dissolving the appropriate amount of solid in Milli-Q water, and the pH was adjusted when required. All pH measurements were undertaken using an Orion glass combination pH electrode connected to a Cybersan 2500 pH meter. The pH electrode was calibrated at room temperature (20 °C) by employing two standard calibration buffers (Orion) prior to solution measurements. All polyethylene storage containers were soaked overnight in dilute hydrochloric acid (1 M) followed by rinsing with large volumes of Milli-Q water. Based on an EDTA-salicylate-ethylenediamine buffer system, the seawater ligand mimetic calibration system was prepared according to the recipe proposed by De Marco and Martizano [18]: 10^{-4} M $FeCl_3$; 10^{-4} M Na_2EDTA; 10^{-3} M $CuSO_4$; 1.5 x 10^{-2} M ethylenediamine (EN); 10^{-2} M sodium salicylate; and 0.60 M NaCl. The Fe-EDTA buffer was made according to the following composition: 10^{-4} M $FeCl_3$,10^{-4} M Na_2EDTA and 0.60 M NaCl. The brine solution, otherwise known as the artificial seawater matrix, was prepared in order to reflect the NaCl concentration (0.60 M) of natural seawater. The copper-ethylenediamine (Cu-EN) buffer was prepared using a mixture of 10^{-4} M $FeCl_3$, 10^{-4} M Na_2EDTA, 10^{-3} M $CuSO_4$ and 0.60 M NaCl with variable amounts of EN, as depicted in Table 1. Unless otherwise specified, all seawater samples were collected in pre-washed polyethylene containers from Coogee Beach, Fremantle (Western Australia), and were filtered through a Supor®-200 0.20 μm membrane filter. The alternative calibration system (ACS) was prepared according to the following procedure:10^{-4} M $FeCl_3$, 10^{-4} M Na_2EDTA, 10^{-3} M $CuSO_4$, 5 x 10^{-3} M EN and 0.6 M NaCl.

2.3. EIS

All EIS studies were undertaken on a Princeton Applied Research PARSTAT 2263 portable electrochemical impedance analyzer. Experimental control and data acquisition were performed using a personal computer utilizing the PowerSuite EIS software. All EIS spectra were recorded at an open circuit potential of ± 10 mV rms and a frequency range between 100 kHz-0.1 mHz (unless otherwise specified). Four point data averaging statistics were used in all instances. A conventional three-electrode cell was employed in the EIS studies comprising an iron chalcogenide glass rotating disc electrode (RDE) [i.e. working electrode], a platinum counter electrode, and a silver/silver chloride Orion double junction (900001) reference electrode. The counter and reference electrodes were cleaned prior to use by rinsing with copious amounts of Milli-Q water and ethanol. For all experiments, the membrane surface of the RDE was cleaned and polished according to the method described above. The RDE was inserted into a single element Pine Instrument Company analytical rotator and rotated at 3000 rpm (unless otherwise specified). All EIS spectra were fitted to equivalent circuits using the equivalent circuit program ZView.

2.4. CFA Potentiometry

2.4.1. Sample Preparation

After preparation of the appropriate iron(III) calibration solution, it was acidified to pH 1 using hydrochloric acid (32 %) and stored for a 1 day before use, in order to improve the stability of the solution and the concomitant response of the electrode. The pH was adjusted between pH 5-9.5 using analytical grade sodium hydroxide, so as to provide a pFe range of 10 to 23, which encompasses the typical pFe value of seawater. The solutions were subsequently allowed to equilibrate at each pH for 30 minutes. The free iron(III) levels at the specific equilibrium pH values were calculated using the MINTEQA2 Academic Version 1.50 equilibrium speciation software, obtained from Allison Geoscience Consultants Inc. It

should be noted that the ISE was polished prior to the measurement of every new potentiometric response curve in calibration standards together with the subsequent analysis of seawater.

2.4.2. CFA Analysis

A flow cell obtained from Chem Flow Devices (Melbourne, Australia) was employed in the CFA of the iron chalcogenide ISE. The flow cell has a standard wall jet design that can accommodate a normal sized and flat-ended ISE. A solid-state silver/silver chloride reference electrode encompassing an anodized silver wire in chloride media was built into the device. An Autoclude (Model VTL) peristaltic pump was utilized to continuously transport two streams of solution through the flow cell at a rate of 3 mL $min.^{-1}$. The stream containing either the iron(III) calibration buffer or seawater sample passes directly below the ISE contacting the membrane surface in the process, whilst the reference solution (0.60 M KCl) traverses the side of the device where it comes into contact with the Ag/AgCl reference electrode. The two solution streams subsequently merge before leaving the flow cell as waste, as represented in Figure 1. All connections in the CFA manifold were made using Ismatec tygon tubing (0.0449” or 1.14 mm I.D). Potential measurements were performed by connecting the ISE and reference electrode to a National Instruments LabPC 1200 A/D board programmed with LabView (version 5.1).

2.5. SR-XPS

After polishing, the membranes were rinsed with large amounts of Milli-Q water followed by ethanol prior to blotting dry on a tissue. These pieces of membrane were subsequently exposed to solution to investigate the surface chemistry of the membrane in various saline solutions. Chips of the polished chalcogenide membrane were soaked in each of these solutions for a total of 24 hours. These fragments were removed from solution and dried under a steady stream of nitrogen gas.

SR-XPS analysis was undertaken at incident beam energies of 400, 170, 1253.6 and 170 eV, respectively, corresponding to the C(1s), Ge(3d), Sb(3d) and survey scans together with Se(3d) XPS spectral regions. A pass energy of 5 eV, dwell time of 0.1 s and energy step of 0.1 eV were used. The C(1s) region arising from adventitious hydrocarbons (binding energy of 284.6 eV) was selected as an internal reference for the detection and correction of surface charging. The remaining regions were specifically targeted to observe changes in the membrane composition following the exposure to solution.

SR-XPS was conducted using the soft X-ray beamlime (14ID) at the Australian Synchrotron (Melbourne). The chalcogenide samples were all mounted onto a stainless steel sample holder using double-sided conductive carbon tape, and introduced to the load lock chamber of the X-ray spectroscopy end station maintained at a pressure of 10^{-7} hPa. Both the beamline and analyser chamber were maintained under ultra-high vacuum (UHV), with the pressure of the analysis chamber at 10^{-10} hPa or better. The insertion device for the beamline is an elliptically polarized undulator (Apple II) capable of producing an energy range of 100-2500 eV with a resolution between 5,000 and 10,000 ($\Delta E/E$). The end station was constructed by OmniVac and PreVac, and equipped with a SPECS Phoibos 150 Hemispherical Analyzer complete with a retarding grid analyzer. The data was acquired by SpecsLab 2.32-r11458 software (SPECS GmbH).

2.6. NEXAFS Spectroscopy

NEXAFS spectroscopy was also conducted on the soft X-ray beamline (SXR, 14ID) of the Australian Synchrotron. The beamline was equipped with an Apple II undulator, which was set to output horizontally polarized light that was then passed through a Peterson plane grating monochromator (1200 lines mm^{-1}). NEXAFS spectra were recorded using a SPECS Phoibos 150 Hemispherical Analyzer incorporating an extended 9 channel detector. The spectra were acquired for both the carbon (275-335 eV) and iron (700-730 eV) K-edge in the partial electron yield, total fluorescence yield and total electron yield (drain current) modes. The data was acquired by SpecsLab 2.32-r11458 software (SPECS GmbH).

3. Results and Discussion

This study utilized a multi-technique approach to develop an improved calibration system, which was expected to provide enhanced electrochemical potentiometric response characteristics and more robust electroanalyses of free iron(III) in natural seawater. First, the powerful electrode kinetic technique of EIS was used to ascertain and match the electrode kinetics of the iron chalcogenide glass ISE between seawater and new seawater ligand mimetic systems, so as to develop a superior calibration buffer. Second, CFA potentiometry has been utilized to confirm that an alternative calibration system generated improved electrochemical behaviour, thereby providing irrefutable evidence of the viability of the optimized calibration buffer. Finally, SR-XPS and NEXAFS were used to probe the modified surface layer (MSL) of the electrode, and characterize the surface reaction products following exposure of membranes to various calibration media and seawater. In particular, SR-XPS and NEXAFS were used as comparative tools to confirm that the optimized calibration system imitates the surface chemistry of the iron(III) sensor in seawater, by contrasting the surface reaction products of the electrode upon exposure to both media. Ultimately, this conglomeration of information allowed the development and optimization of a new and improved seawater ligand mimetic calibration system.

A RDE is one of the most accessible and well-known hydrodynamic electrodes comprising a disk containing the electrode material (i.e. $Fe_{2.5}(Se_{60}Ge_{28}Sb_{12})_{97.5}$) embedded in a rod of an insulating sheath [20, 21]. The assembly can be rotated about an axis perpendicular to the surface of the electrode [20]. The motion of the electrode leads to a very well defined solution flow pattern. The imposition of convection following rotation of the electrode leads to an increase in the rate of mass transfer, which results in a decrease of the diffusion layer thickness triggering an enhanced electrochemical response [20, 21]. The effective thickness of the diffusion layer is governed by the Levich equation and is dictated by a multitude of factors including the kinematic viscosity, concentration of electroactive species in bulk solution and rotation speed [22]. EIS spectra were fitted to the equivalent circuit embodying

a solution resistance (R_{SOLN}) and charge transfer resistance (R_{CT}) in parallel with a constant phase element (Q_{CT}), yielding the circuit element values presented in Table 2.

Theoretically, a plot of log($1/R_{CT}$) against log(rotation speed) should provide a linear relationship with a slope of 0.5, in accordance with the Levich equation for a RDE [22] that takes account of thinning of the electrode diffusion layer as a function of rotation speed together with acceleration of the rate of semi-infinite linear diffusion and its concomitant facilitation of the rate of this diffusion-controlled charge transfer reaction. In this instance, a plot of log($1/R_{CT}$) versus log(rotation speed) yielded a slope of 0.4 (see Figure 2a), which is close to the expected value of 0.5 in the Levich equation. The slight deviation in the slope can be attributed to the experimental error due to electrode instability during EIS measurements with ISEs, noting that previous research has demonstrated that this experimental error is of the order of ±10-20% relative [23]. This demonstration is critically important in using EIS in elucidation of the electrode kinetics of the iron chalcogenide glass ISE in seawater and seawater ligand mimetic calibration buffers, as it instils confidence in a utilization of the theoretical and experimental aspects of EIS in a matching of the matrix effects of seawater and calibration systems on the response of the iron(III) ISE. Furthermore, the RDE studies showed that the Warburg diffusion impedance of the Fe(III) ISE is suppressed substantially at 3000 rpm, thereby allowing observation of the low frequency EIS response that is attributable to R_{CT}.

3.1. Seawater Ligand Mimetic System

The central issue which has plagued the use of the iron(III) chalcogenide ISE in contemporary times has been the lack of a suitable calibration system for the electroanalysis of iron(III) in seawater [10]. The problem lies in the fact that artificial seawater matrices are incapable of simulating the surface chemistry and concomitant potentiometric response characteristics of the ISE, so as to enable reliable determinations of the free iron(III) activity in seawater [10]. A recent paper by De Marco and Martizano [18] endeavoured to simulate the influence of ubiquitous organic ligands in seawater by trialling a blend of different

synthetic ligands that comprise the same functionalities as the organic ligands of seawater. The combined buffer system was termed a seawater ligand mimetic system, and was shown to provide a near-Nernstian potentiometric response that is capable of yielding reasonable electroanalyses of free iron(III) in seawater [18]. Expectedly, the response of the iron(III) ISE in this calibration system was rapid and stable, and the electrode response slope correlated well with the expected Nernstian behaviour of this electrode [18].

3.2. Calibration Issues

Figure 3a presents the EIS Nyquist plot for an iron(III) chalcogenide RDE in the ACS medium. The data revealed the presence of three time constant elements, which are depicted as semi-circles in the Nyquist plot. The small semi-circle at high frequency (extreme left) is ascribable to the formation of a thin surface film known as the outer surface layer (OSL) [23]. The second semi-circle in the medium to low frequency region (next region down) is indicative of an iron deficient modified surface layer (MSL) which is ~20 nm in thickness [23]. It is widely proposed that the potential generating process of the chalcogenide glass electrode is governed by the formation of an MSL, where it is believed that this MSL facilitates ion-exchange [24]. The larger time constant at lower frequency (extreme right) is attributable to a coupling of the double layer capacitance of iron(III) ISE and the charge transfer resistance at the electrode/electrolyte interface [23]. Figure 2b shows the equivalent electrical circuit fitted to the impedance response of the iron chalcogenide glass RDE. The equivalent circuit parameters for a RDE chalcogenide iron(III) ISE in the seawater ligand mimetic system (included for comparison), ACS and seawater are presented in Table 3. Based upon the EIS data, it is evident that the dielectric properties of the RDE corresponding to various time constants differ significantly between the two systems. Previous research by De Marco and Pejcic [23] demonstrated unambiguously that the response mechanism of the Fe(III) ISE is based on a combination of ion exchange and charge transfer occurring at the electrode/electrolyte interface, with the kinetics of these reactions depicted by the charge transfer impedance (i.e. R_{CT}) and the impedance of the modified surface layer (i.e. R_{MSL}). It is important to note that this combined ion-exchange process with an independent slope of

$\frac{2.303RT}{3F}$ or 19.72 mV decade^{-1} coupled with the one electron charge transfer reaction with a separate slope of $\frac{2.303RT}{F}$ or 59.17 mV decade^{-1} equalizes at identical electrode reaction sites on a uniform ISE surface, yielding a net or overall Nernstian slope of $\frac{2\times2.303RT}{4F}$ or 29.59 mV decade^{-1} at 25 ^{o}C [23]. Figure 3b represents the Nyquist plot for the Fe(III) RDE in seawater. It is significant to note that natural seawater yielded similar R_{OSL} and R_{MSL} values when compared to that of the seawater ligand mimetic system. However, a large positive difference in R_{CT} was observed between the seawater ligand mimetic system and natural seawater, with the diminution in the rate of this process showing that the natural organic ligands of seawater are impeding the charge transfer process at the ISE surface. In any event, the fact that the R_{CT} for the kinetic parameters is significantly different in the calibration system and natural seawater demonstrates that matrix matching of seawater and the calibration buffer system is imperfect. The data in Table 3 indicates that the seawater ligand mimetic system proposed by De Marco and Martizano [18] is unable to simulate exactly the fundamental electrode kinetics of the iron(III) chalcogenide ISE in seawater. Accordingly, the EIS data highlight the need for the development of improved calibration and measurement protocols for use with this sensor.

3.3. Fe-EDTA Buffer

The main hypothesis of this study is that an improved calibration system may be developed by trialling different permutations of synthetic ligands that are representative of the functionalities of natural ligands in seawater. A series of blends of synthetic ligands were tested initially; however, preliminary studies revealed an ambiguity in the response observed comparative to the seawater ligand mimetic system. In particular, the raw CFA response data of the seawater ligand mimetic system minus sodium salicylate (a key component of this buffer [18]) provided essentially the same potentiometric response as the seawater ligand mimetic system. This response is unusual considering that the different synthetic ligands have varying critical stability constants (K_{stab}) for iron(III) {viz., $logK_{stab}[Fe(III)\text{-}EDTA]$ =

25.0 and $logK_{stab}$*[Fe(III)-salicylate]* = 15.81 [23]}, and should lead to a variation in the iron(III) speciation in the buffer and the concomitant response of the calibration system. Nevertheless, this uncharacteristic electrochemical response compelled us to revert to the original seawater ligand mimetic system, and explore the role of each component in the system to further understand the behaviour of this complex medium. Consequently, we initially examined the Fe-EDTA buffer system comprising 10^{-4} M $FeCl_3$, 10^{-4} M Na_2EDTA and 0.60 M NaCl.

Since aminopolycarboxylates have a tendency to adsorb tenaciously to ISE surfaces yielding erroneous potentiometric response characteristics [25-29], this study has utilized a non-standard 1:1 molar mixture of Fe(III) and EDTA, so that with low aFe^{3+} values in the buffer (i.e., pFe =10-23), there would be negligible amounts of reactive EDTA species to adsorb to and foul the electrode surface. Accordingly, the iron complexation equilibria in this buffer system are heavily influenced by the solution pH in the absence of a typical excess of EDTA ligand.

The equivalent circuit presented in Figure 2b was also used to model the EIS data depicted in Figure 3(c), and the corresponding circuit parameters are summarized in Table 3. A comparison of the equivalent circuit parameters presented in Table 3 revealed a 2-fold increase in the R_{MSL} value when the electrode is immersed in the EDTA buffer solution compared to natural seawater. The drastic increase in the impedance of the MSL shows that EDTA inhibits the ion exchange of iron(III), which is most likely due to the formation of a metal organic film, as proposed above. Furthermore, an elevation (33% relative) was observed in the impedance of the high frequency time constant corresponding to the outer surface layer. A much higher R_{OSL} level was observed in the electrode exposed to the EDTA buffer, indicating a significant decrease in the linear diffusion of Fe(III) into the electrode. Whatever the reason, it is evident from comparison of the equivalent circuit parameters of the iron(III) sensor in both systems and the ISE potentiometric response characteristics that the EDTA buffer is incapable of simulating the electrochemical and surface chemistry effects of ubiquitous organic ligands in seawater.

The CFA response data for the chalcogenide Fe(III) ISE in the saline EDTA buffer is presented in Figure 4a and its calibration plot in Figure 4b. It is important to note that the CFA response required a longer time to achieve a steady state potential (~ 15 minutes), which is consistent with previous research indicating that single ligand metal ion buffers comprising EDTA yield an extremely sluggish response [25]. The electrode slope for the chalcogenide ISE in the saline EDTA buffer is 9.72 mV decade^{-1}, which is markedly different from the theoretically expected value of 29.6 mV decade^{-1} [23]. As stressed earlier, the anomalous sub-Nernstian response observed in the Fe-EDTA buffer is comparable to the unusual electrochemical behaviour found with the copper ($Cu_{1.8}Se$) ISE in the presence of EDTA and cadmium sulfide-based ISEs in the presence of a range of different aminopolycarboxylates [25, 26]. It has been proposed that an abnormal potentiometric response with solid-state ISEs in EDTA can be attributed to the formation of a tenacious metal-organic film that ultimately affects the electrode response [27-29].

3.4. Cu-EN/Fe-EDTA Buffer

Previous research conducted by De Marco and Martizano [18] suggested that copper(II) complexes were a pre-requisite in the seawater ligand mimetic calibration system, in order to simulate the iron phase crystallization chemistry of the sensor. As a result, it was theorized that the addition of both copper(II) and ethylenediamine to the pre-existing Fe-EDTA buffer may drastically enhance the electrochemical response.

The CFA response data and corresponding Nernstian response curve for the electrode in the Cu-EN/Fe-EDTA mixture is presented in Figure 5a and corresponding calibration plot in Figure 5b. It is evident that the iron(III) ISE yields a Nernstian response slope of 28.30 mV decade^{-1}, which is commensurate with the theoretical value derived theoretically by De Marco and Pejcic [23] based on a combination of ion exchange and charge transfer at the electrode/electrolyte interface (29.6 mV decade^{-1}). The significant disparity observed in the response of the iron(III) ISE in the EDTA buffer and the following calibration system can

ultimately be attributed to the presence of Cu(II) ions or the concomitant bis(ethylenediamine) copper(II) complex. A recent study undertaken by Ishikawa et al. [30] on the corrosion of iron revealed that trace amounts of Cu(II) ions can alter the products of iron corrosion and promote the formation of smaller crystallites [30]. In particular, Cu(II) ions were shown to promote the formation of pure Fe_3O_4, by interfering with the production of the most stable iron corrosion product (i.e. α-FeOOH). In any event, the anti-corrosive characteristics associated with Cu(II) on iron, in principle, may be applicable to the inhibition of oxidative dissolution of the iron chalcogenide ISE. Based on the experimental results and previous corrosion studies, the aforementioned buffer composition formed the framework for the development of the improved calibration system.

3.5. Optimization of the Seawater Ligand Mimetic Calibration System

Despite the pronounced improvement in the potentiometric response characteristics and concomitant electrochemical response for the Cu-EN/Fe-EDTA seawater ligand mimetic system, previous in situ EIS/SR-GIXRD data [17] showed that the matching of matrix effects was imperfect, so there was scope for significant improvement. As it was previously demonstrated that copper(II) is a key ingredient in the system, which accounted for the improved response of this system, it was proposed that an alteration of the composition of copper and ethylenediamine might allow a regulation of the free copper(II) concentration, with a view to fine-tuning and optimizing the influence of these species in the calibration system.

The EIS Bode phase plot presented in Figure 5c was used to investigate the high frequency (i.e. ~ 10 kHz–100 Hz) and low frequency response (i.e. 100-0.1 mHz) of the RDE. It is evident that the buffer system employing a molar composition of 1:5 (copper(II): ethylenediamine) yielded an near-perfect simulation of the high-to-moderate frequency response in seawater. Significantly, this system's close EIS response of the high frequency data in seawater, which are attributable to the kinetic parameters ascribable to the OSL and MSL, suggests that this calibration solution might be a viable calibration system for the

electroanalysis of free iron(III) in seawater. However, it should be noted that the significant disparity in low frequency response ascribable to the charge transfer resistance (i.e., R_{CT}) of seawater and the ACS buffered medium is due to a difference in the free iron(III) activity in the ACS set at a different pH (i.e., 5) and pFe (i.e.,12), as calculated using MINTEQA2 in the ACS), and its concomitant facilitation of the charge transfer research or diminution in R_{CT} of the electrode.

The iron(III) calibration buffers are pH regulated via deprotonation/protonation of the complexation ligands, thereby altering the free iron(III) activity (i.e., pFe) in the media and the concomitant R_{CT} value at low frequency, noting that previous research by De Marco and Pejcic [23] showed that the net rate of the charge transfer reaction (reflected by R_{CT}) is altered dramatically at different values of pFe. Hence, it was essential that the pH of this buffer was adjusted to give an identical pFe value to that of natural seawater (i.e., pFe ~ 21). Accordingly, the Bode phase plot of natural seawater against the alternative calibration system (ACS) at pFe = 21 (at pH ~ 8.5) is shown in Figure 5d.

As evident in Figure 5d, the ACS is capable of replicating both the high frequency and low frequency response of seawater, as illustrated by the excellent correlation between the EIS responses of R_{OSL}, R_{MSL} and R_{CT} (see Table 3). By comparison of the dielectric properties of the RDE exposed to both natural seawater and the ACS, it is evident that the interfacial properties of the chalcogenide glass membrane are almost identical in seawater and the ACS. The slight discrepancy in R_{OSL} and R_{CT} of 1-10% is commensurate with the repeatability of the EIS method, while the larger deviations in R_{MSL} is probably due to inaccuracies associated with equivalent circuit fitting when a medium value of medium frequency resistance is deconvoluted from significantly larger values of low and high frequency resistances (i.e., R_{OSL} and R_{CT}) yielding a higher experimental error of ~ 20-30 %. Nevertheless, the slight discrepancies in the dielectric properties of the RDE exposed to both systems are most likely ascribable to the experimental uncertainty rather than a significant difference in the response attributes of the iron chalcogenide glass ISE in seawater and the ACS. Clearly, the similarity in the interfacial kinetics of the iron chalcogenide glass RDE in seawater and the ACS, as

evidenced by the comparability of R_{OSL}, R_{MSL} and R_{CT} values (see Table 3), confirms that the ACS is capable of simulating effectively the electrochemical effects of ubiquitous seawater organic ligands on the electrode response characteristics of the iron chalcogenide glass ISE.

3.6 Electroanalysis of Iron(III) in Seawater

Figure 6a and 6b depict CFA and potentiometric response calibration curve, respectively, for an iron(III) chalcogenide ISE in the seawater ligand mimetic calibration system proposed by Martizano and De Marco [18]. The response of the iron(III) ISE is rapid and stable in this calibration medium, and the electrode response slope of 32.60 ± 0.2 mV decade^{-1} compares favourably with the theoretically expected Nernstian response of 29.60 mV/decade. A comparison of six replicate analyses of seawater against the Nernstian response curve for the calibration standards yielded values of log[aFe^{3+}] = -20.06 ± 0.11, with the reported variance representing the standard deviation in these six replicates. The value of free iron(III) determined in seawater compares favourably with recent experimental data, which suggests that free iron(III) concentrations in natural seawater can range from pFe_{Free} = 19.5-21.2 [31].

Figure 6c presents the CFA potentiometric response curve for the iron(III) ISE in the new ACS system. It is evident from the monotonic response of the electrode that steady-state potentials are achieved in a relatively short period of time, following stepwise changes in the activity of Fe(III) in the various calibration standards. Also evident in the data in Figure 6d is that the iron (III) ISE immersed in the alternate calibration system yielded a near-perfect Nernstian response of 28.82 ± 0.16 mV decade^{-1}. Using this potentiometric calibration curve, six replicate CFA analyses of seawater using the iron (III) ISE yielded log[aFe^{3+}] values of -20.46 ± 0.12. Again, the level of free iron(III) in seawater, as measured against the ACS, is commensurate with the predicted speciation model for iron(III) complexed by natural organic ligands in seawater [31].

Herein, it was deemed necessary to ascertain if the ACS buffer provided improved potentiometric determinations of the iron chalcogenide glass ISE in natural seawater. An

independent t-test was used to evaluate if a statistical disparity exists between the log[aFe^{3+}] of seawater (dependent variable) obtained via the seawater ligand mimetic calibration system and the ACS (independent variable). These levels of iron(III) in seawater obtained from the seawater ligand mimetic system (M = -20.06, SD = 0.11) are statistically dissimilar to the levels of iron(III) obtained using the ACS (M = -20.46, SD = 0.12), t(10) = 5.916, p = 0.00015. Significantly, the determined *t* value at the 95 % confidence level for 10 degrees of freedom ($N_1 + N_2$ - 2) of 5.916 greatly exceeds the tabulated *t* value of 2.228, thereby confirming the null hypothesis that there is a significant difference in the pFe values obtained using the two calibration systems at a 95 % confidence level.

Moreover, effect size statistics can provide an indication of the magnitude of the differences between groups of data. There are a number of different effect size statistics, with the most common one involving η^2 [32]. The η^2 values range from 0 to 1, and represent the proportion of variance in the dependent variable that can be explained by the independent variable [32]. The formula used for calculating η^2 is given below:

$$\eta^2 = t^2/[t^2+(N_1 + N_2 -2)]$$
$$\eta^2 = 5.9162^2/[5.9162^2 + (6 + 6 -2)] = \underline{0.778}$$

The guidelines proposed by Cohen for interpreting the η^2 value are roughly given by: 0.01 = small effect; 0.06 = moderate effect; 0.14 = large effect [32]. In this particular instance, the effect size of 0.778 is very large, confirming that there is a significant deviation in the log[aFe^{3+}] values of the two calibration media. Consequently, statistical analysis has demonstrated that the ACS yielded improved electroanalyses of iron(III) in seawater relative to the previously proposed seawater ligand mimetic system of Martizano and De Marco [18].

3.7 SR-XPS

The ability of the ACS system to simulate the surface chemistry effects of seawater on the iron chalcogenide glass ISE was investigated by SR-XPS. Information pertaining to the

surface reaction products was obtained by examining in detail the binding energies, intensities and shapes of the XPS peaks. Table 4 summarizes the binding energies of the species detected, noting that the polished untreated membrane was used as a control and included for comparison. It is important to note that a detailed interpretation of the XPS data for the chalcogenide membrane treated in the brine solution and citrate buffer will not be reported herein, as previous mechanistic studies have already confirmed that these saline solutions are poor calibration matrices because they totally destroy the ISEs MSL [17].

As depicted by Table 4, XPS was able to identify the presence of three different carbon species. The two peaks at lower binding energies (i.e. 285.0, ~ 286.5 eV) are attributable to contamination from the analysis chamber of the instrument via adventitious hydrocarbons together with alcohol from the rinsing of the membranes during polishing [33]. The third peak at ~288.7 eV was only identified following solution exposure of the membrane to natural seawater, and is consistent with the presence of a carbonate or carboxylate species. Moreover, the broad unresolved nature of the peak is symbolic of carbon in a myriad of different chemical environments (i.e. phenols, carboxylic acids, esters etc.). Ultimately, the following observations are indicative of the surface adsorption of seawater's natural organic ligands onto the membrane. This is commensurate with the notion proposed by De Marco et al. [17] that the ubiquitous organic ligands (i.e. humates and fulvates) preferentially adsorb to the surface crystalline phases of the sensor, thereby inhibiting their destruction via oxidative dissolution. Further credence for this proposed theory was attained upon detection of nitrogen, which also indicates bonding between the natural organic ligands and the chalcogenide surface is facilitated via inherent nitrogenous functional groups (i.e. amides, amines etc.). Moreover, the N(1s) peak at 400.0 eV (see Figure 7a) is indicative of amine nitrogens from the organic ligands [33].

A high resolution SR-XPS spectrum collected on the Fe(2p) level (not shown) revealed that XPS failed to detect any iron in the surface region of all the treated membranes, with a lack of iron detection in the surface region attributable to the iron deficient modified surface layer (MSL) of the ISE.

The Ge(3d) spectra for the chalcogenide membrane exposed to seawater revealed the presence of a broad peak indicative of numerous germanium species. High resolution spectra for the Ge(3d) level of the ACS and seawater treated membranes revealed broad peaks indicative of several germanium species. The positions of the broad peaks (about 30.5 eV) is consistent with germanium in the form of GeSe or $GeSe_2$. The appearance of a high binding energy shoulder at 32.1 eV are also attributable with the presence of a GeO_2 species [33, 34]. In summary, a near identical Ge surface chemistry was observed with the iron chalcogenide glass membrane conditioned in the ACS as compared to seawater.

The binding energies of Sb(3d) levels for the iron chalcogenide glass membrane exposed to various saline solutions are also presented in Table 4. The Sb(3d) spectrum for a polished chalcogenide membrane revealed $Sb(3d_{5/2})$ and $Sb(3d_{3/2})$ spin-orbit coupled components at 529.7 and 539.1 eV respectively. The positions of these peaks are attributable to Sb_2Se_3/Sb_2O_3 [33]. By contrast, conditioning of the membrane in the ACS system resulted in the formation of broad high energy binding shoulders on the Sb(3d) peaks at 530.9 and 540.2 eV, which signify the presence of Sb_2O_5 or $Sb(OH)_5$ [33]. It is worth noting that a significant increase in intensity was observed in the O(1s) peak (not shown), which is consistent with the formation of a Sb_2O_5 or $Sb(OH)_5$ species. As a result, it is proposed that the ACS matrix facilitates a surface oxidation reaction, similar to that observed with germanium. It should be noted that the Sb(3d) spectra (not shown) in both seawater and ACS treated membranes were practically indistinguishable also signalling a near identical Sb surface chemistry for the Fe(III) ISE membrane in both the ACS and seawater.

The $Se(3d_{5/2})$ and $Se(3d_{3/2})$ spin-orbit split components at about 53.9 eV and 54.7 eV (see Table 4), respectively, are indicative of Se in selenides such as GeSe, $GeSe_2$, FeSe, etc. [33], with the high binding energy shoulder at approximately 55.4 eV for solution treated membranes consistent with elemental selenium arising from oxidation of selenide, as observed by De Marco and Pejcic [23]. Although the Se(3d) spectra are not shown herein, it should be noted that the peak ratios for unoxidized and oxidized Se and the concomitant peak

shapes were matched between the ACS and seawater treated surfaces, but not for any of the other membranes. This is also shows that there is a matching of matrix effects on the Fe(III) ISE membrane surface chemistry in the ACS and natural seawater.

In conclusion, it has been established that aging of the membrane in the ACS yielded comparable Sb(3d), Ge(3d) and Se(3d) SR-XPS spectra relative to the seawater treated membrane. This observation reaffirms the notion that the ACS is capable of simulating effectively the surface chemistry effects of natural seawater organic ligands on the ISE membrane. These observations add significant credence to the suitability of the ACS system for the electroanalysis of iron(III) in seawater.

Interestingly, it should also be noted that copper was detected on the membrane surface of the electrode subjected to the ACS system (see Table 4). The Cu($2p_{3/2}$) and Cu($2p_{1/2}$) spin-orbit split components yielded single peaks at 932.7 eV and 952.5 eV, which are consistent with the presence of Cu(I) [33]. The fact that copper was detected on the membrane surface, corroborates the notion that Cu is altering the crystallization chemistry of Fe(III)-hydroxide phases formed at the surfaces of oxidized iron based materials, thereby allowing a matching of the effects by natural seawater ligands and the ACS matrix on the response of the iron chalcogenide glass ISE [30].

3.8 NEXAFS Spectroscopy

To corroborate the aforementioned hypothesis on the influence of copper in the ACS on the iron surface phases on the Fe(III) ISE, it has been necessary to utilize a surface science technique with a sufficient analytical sensitivity and ability for structure elucidation in the identification of iron at the Fe(III) ISE membrane surface in the ACS and seawater. In this context, NEXAFS spectroscopy of the Fe(2p) or K-edge was studied, so as to bring about a significant increase in the Fe(2p) photoabsorption cross section and detection limit by orders of magnitude, also noting that NEXAFS yields critical chemical state information since the ejected photoelectrons undergo inelastic scattering with neighbouring iron atoms during

Fe(2p) photoionization giving rise to characteristic fine structure in the NEXAFS spectra. The NEXAFS Fe(2p) spectrum of the untreated or control chalcogenide membrane (see Figure 7b) displayed a sharp and intense Fe($2p_{3/2}$) peak at 708.0 eV and a weaker partially resolved peak at approximately 710.5 eV, which are distinctive for Fe(II) [35, 36]. This is internally consistent with a chalcogenide membrane that has been doped with iron(II) during the fusion of iron(II) selenide into the membrane. On the other hand, the membranes that have been conditioned in both seawater and ACS, exhibited a weaker and less intense Fe($2p_{3/2}$) peak at 707.9 eV with a major and sharp peak at 709.6 eV, which is commensurate with iron in the form of Fe(III) [35, 36]. Although the results are not shown here, the authors' previous study [37] demonstrated that exposure of the iron chalcogenide glass ISE to other iron calibration standards such as brine and saline citrate buffer yielded a mixture of Fe(III) and Fe(II) in the MSL of the electrode. Hence, the ACS and seawater only yield Fe(III) in the MSL, and this is a key reason as to why the ACS is a good simulator of the surface chemistry effects of seawater on the iron chalcogenide ISE in seawater.

4 Conclusions

This study led to the development of an improved calibration system for the iron(III) chalcogenide ISE, providing a means for the accurate and reliable electroanalysis of iron(III) in seawater. The previously prepared seawater ligand mimetic calibration system of Martizano and De Marco [18] was only capable of partially simulating the surface and electrochemical effects of natural organic ligands on the iron chalcogenide glass ISE. Herein, EIS and CFA-ISE potentiometry have demonstrated unequivocally that an ACS comprising a mixture of 10^{-4} M $FeCl_3$, 10^{-4} M Na_2EDTA, 10^{-3} M $CuSO_4$, 5 x 10^{-3} M EN and 0.60 M NaCl yields an improved electrochemical response as compared to the previously published calibration system of Martizano and De Marco [18]. Importantly, calibration of the iron chalcogenide glass ISE in the ACS provided a Nernstian response of 30 mV $decade^{-1}$ according to the known ion-exchange/electron transfer response mechanism of this ISE, and electroanalyses of iron(III) in seawater using the ACS system yielded pFe values consistent with recent literature data for the speciation of iron(III) in seawater. Moreover, the seawater

ligand mimetic and ACS systems yielded statistically significant differences in log[aFe^{3+}] values in seawater, demonstrating that the ACS system provides an improved electrochemical response in seawater. Most significantly, the effectiveness of the ACS in simulating the surface chemistry effects of the seawater matrix on the iron(III) ISE membrane has been corroborated by comparative EIS, SR-XPS and NEXAFS studies of the membrane in the ACS and natural seawater.

5. Acknowledgements

Financial support from the Australian Research Council (Projects LX0776015 and DP0987851) is gratefully acknowledged. Part of this work was undertaken on the soft X-ray spectroscopy beamline at the Australian Synchrotron (AS), Victoria, Australia. We are very grateful to Dr. Bruce Cowie and Dr. Anton Tadich at the AS for assistance and advice in the running and interpretation of SR-XPS and NEXAFS spectra.

6. Vitae

Mark Maric was born in Melbourne, Australia. He received his BSc Forensic and Analytical Chemistry degree from Curtin University, Australia. He is currently conducting his Doctor of Philosophy studies at Curtin University. His main research focus and interests involve the analysis and characterization of forensic trace evidence and the use of chemometrics in the interpretation of spectroscopic data.

Manzar Sohail was born in Mandra, Pakistan. He received his M.Sc. Chemistry degree from Government College Lahore and M.Phil. in Inorganic Chemistry from Quaid-i-Azam University, Pakistan. He obtained his PhD at Monash University, Australia in October 2009. During his postdoctoral appointments he worked at the Nanochemistry Research Institute, Curtin University and University of the Sunshine Coast, Australia. His main research focus and interest is fabrication of electrochemical sensors, synthesis of new electrode surfaces and surface characterization techniques particularly X-ray photoelectron spectroscopy. Currently,

he is a Research Scientist at the Center of Excellence for Nanotechnology, King Fahd University of Petroleum and Minerals, Saudi Arabia.

Jean-Pierre Veder was born in Perth Australia. He was awarded his Bachelor of Science (Nanotechnology) with First Class Honours in 2006 from Curtin University, Australia, and subsequently received his PhD in 2010 from Curtin University. He has been an Office of the Chief Executive (OCE) Postdoctoral Research Fellow at the Commonwealth Scientific Industrial Research Organization (CSIRO) since 2010. His main research focus and interests are in ionic liquids particularly using a wide array of spectroscopic and materials characterization techniques in the elucidation of the mechanistic chemistry of applied electrochemical systems harnessing these ionic liquid electrolytes.

Roland De Marco was born in Melbourne, Australia. He received his PhD in 1992 from La Trobe University, Australia. He was a Research Scientist at CSIRO, Australia (1990-1992), Lecturer in Chemistry at University of Tasmania, Australia (1992-1995) before moving to Curtin University, Australia in 1995. He worked his way up the ranks at Curtin University culminating with his appointment as Associate Deputy Vice-Chancellor (Research Strategy) in 2010 before taking up his present position in 2011of Pro Vice-Chancellor (Research) at University of the Sunshine Coast, Australia. His main research interests are electrochemical surface and interface analysis, electrochemical sensors and fuel cells.

7. References

[1] W.G. Sunda, Bioavailability and Bioaccumulation of Iron in the Sea; The biogeochemistry of Iron in Seawater, in: D.R. Turner, K.A. Hunter (Eds.) The Biogeochemistry of Iron in Seawater, John Wiley and Sons, West Sussex, 2001, pp. 41-50.

[2] J.H. Martin, K.H. Coale, K.S. Johnson, S.E. Fitzwater, R.M. Gordon, S.J. Tanner, C.N. Hunter, V.A. Elrod, J.L. Nowicki, T.L. Coley, R.T. Barber, S. Lindley, A.J. Watson, K. Van Scoy, C.S. Law, M.I. Liddicoat, R. Ling, T. Stanton, J. Stockel, C.

Collins, A. Anderson, R. Bidigare, M. Ondrusek, M. Latasa, F.J. Millero, K. Lee, W. Yao, J.Z. Zhang, G. Friederich, C. Sakamoto, F. Chavez, K. Buck, Z. Kolber, R. Greene, P. Falkowski, S.W. Chisholm, F. Hoge, R. Swift, J. Yungel, S. Turner, P. Nightingale, A. Hatton, P. Liss, N.W. Tindale, Testing the iron hypothesis in ecosystems of the equatorial Pacific Ocean, Nature 371 (1994) 123-129.

[3] K.H. Coale, K.S. Johnson, S.E. Fitzwater, R.M. Gordon, S. Tanner, F.P. Chavez, L. Ferioli, C. Sakamoto, P. Rogers, F. Millero, P. Steinberg, P. Nightingale, D. Cooper, W.P. Cochlan, M.R. Landry, J. Constantinou, G. Rollwagen, A. Trasvina, R. Kudela, A massive phytoplankton bloom induced by an ecosystem-scale iron fertilization experiment in the equatorial Pacific Ocean, Nature 383 (1996) 495-501.

[4] K. Güssow, A. Proelss, A. Oschlies, K. Rehdanz, W. Rickels, Ocean iron fertilization: Why further research is needed?, Mar. Policy 34 (2010) 911-918.

[5] R. De Marco, B. Pejcic, K. Prince, A. van Riessen, A multi-technique surface study of the mercury(II) chalcogenide ion-selective electrode in saline media, Analyst 128 (2003) 742-749.

[6] J. Wang, Analytical Electrochemistry, John Wiley and Sons, New Jersey 2001.

[7] R. De Marco, Z.-T. Jiang, T. Becker, G. Clarke, G. Murgatroyd, K. Prince, Response multitechnique materials characterization approach, Electroanalysis 18 (2006) 1273-1281.

[8] B. Pejcic, R.D. Marco, C.E. Buckley, C.F. Maitland, R. Knott, A small angle neutron scattering and electrochemical impedance spectroscopy study of the nanostructure of the iron chalcogenide glass ion-selective electrode, Talanta 63 (2004) 149-157.

[9] F.M.M. Morel, N.M. Price, The Biogeochemical Cycles of Trace Metals in the Oceans, Science 300 (2003) 944-947.

[10] R. De Marco, G. Clarke, B. Pejcic, Ion-Selective Electrode potentiometry in environmental analysis, Electroanalysis 19 (2007) 1987-2001.

[11] Y.G. Vlasov, E.A. Bychkov, Chalcogenide glass chemical sensors: Relationship between ionic response, surface ion exchange and bulk membrane transport, J. Electroanal. Chem. 378 (1994) 201-204.

[12] Y.G. Vlasov, E.A. Bychkov, A.V. Legin, Chalcogenide glass chemical sensors: Research and analytical applications, Talanta, 41 (1994) 1059-1063.

[13] A.V. Legin, E.A. Bychkov, Y.G. Vlasov, Analytical applications of chalcogenide glass chemical sensors in environmental monitoring and process control, Sensors Actuat. B-Chem. 24 (1995) 309-311.

[14] R. De Marco, D.J. Mackey, Calibration of a chalcogenide glass membrane ion-selective electrode for the determination of free Fe^{3+} in seawater: I. Measurements in UV photooxidised seawater, Mar. Chem. 68 (2000) 283-294.

[15] R.S. Eriksen, D.J. Mackey, P. Alexander, R. De Marco, X.D. Wang, Continuous flow methods for evaluating the response of a copper ion selective electrode to total and free copper in seawater, J. Environ. Monitor. 1 (1999) 483-487.

[16] R. De Marco, B. Pejcic, X.D. Wang, Continuous flow analysis of iron (III) in seawater using a chalcogenide glass ion-selective electrode, Lab. Robotics Automat. 11 (1999) 284-288.

[17] R. De Marco, Z.-T. Jiang, J. Martizano, A. Lowe, B. Pejcic, A. van Riessen, In situ electrochemical impedance spectroscopy/synchrotron radiation grazing incidence X-ray diffraction—A powerful new technique for the characterization of electrochemical surfaces and interfaces, Electrochim. Acta 51 (2006) 5920-5925.

[18] R. De Marco, J. Martizano, Response of the iron chalcogenide glass membrane ion-selective electrode in a seawater ligand mimetic calibration buffer, Electroanalysis 19 (2007) 2513-2517.

[19] C.E. Koenig, E.W. Graber, Reinvestigation of a ferric ion-selective electrode based on the chalcogenide glass $Fe_x[Se_{60}Ge_{28}Sb_{12}]_{100-x}$(x = 1–10), Electroanalysis 7 (1995) 1090-1094.

[20] A.J. Bard, L.R. Faulkner, Electrochemical Methods: Fundamentals and Applications, 2nd Edition, John Wiley and Sons, New York, 2001.

[21] C.M.A. Brett, A.M.O. Brett, L. Tugulea, Anodic stripping voltammetry of trace metals by batch injection analysis, Anal. Chim. Acta 322 (1996) 151-157.

[22] V.G. Levich, Physicochemical hydrodynamics, Prentice-Hall Inc., Englewood Cliffs, New Jersey, 1962.

[23] R. De Marco, B. Pejcic, Electrochemical impedance spectroscopy and X-ray photoelectron spectroscopy study of the response mechanism of the chalcogenide glass membrane iron(III) ion-selective electrode in saline media, Anal. Chem. 72 (2000) 669-679.

[24] V.S. Vassilev, S.V. Boycheva, Chemical sensors with chalcogenide glassy membranes, Talanta 67 (2005) 20-27.

[25] A. Yuchi, H. Wada, G. Nakagawa, The performance of a cadmium ion-selective electrode in metal buffer solutions and the determination of the stability constants of cadmium complexes, Anal. Chim. Acta 149 (1983) 209-216.

[26] B. Hoyer, Calibration of a solid-state copper ion-selective electrode in cupric ion buffers containing chloride, Talanta 38 (1991) 115-118.

[27] G.J.M. Heijne, W.E. van der Linden, The formation of mixed copper sulfide—silver sulfide membranes for copper(II)-selective electrodes: Part III. The electrode response in the presence of complexing agents, Anal. Chim. Acta 96 (1978) 13-22.

[28] G.J.M. Heijne, W.E. Van Der Linden, G. Den Boef, The formation of mixed copper(II) sulfide—silver(I) sulfide membranes for copper(II)-selective electrodes, Anal. Chim. Acta 89 (1977) 287-296.

[29] W.E. van der Linden, R. Oostervink, The formation and properties of mixed cadmium sulfide—silver sulfide, and mixed mercury sulfide—silver sulfide membranes for electrodes selective to cadmium(II) and mercury(II), Anal. Chim. Acta 108 (1979) 169-178.

[30] T. Ishikawa, H. Nakazaki, A. Yasukawa, K. Kandori, M. Seto, Influences of Co^{2+}, Cu^{2+} and Cr^{3+} ions on the formation of magnetite, Corros. Sci. 41 (1999) 1665-1680.

[31] F.J. Millero, W. Yao, J. Aicher, The speciation of Fe(II) and Fe(III) in natural waters, Mar. Chem. 50 (1995) 21-39.

[32] J. Cohen, Statistical power analysis, Curr. Dir. Psychol. Sci. 1 (1992) 98-101.

[33] J.F. Moulder, W.F. Stickle, P.E. Sobol, K.D. Bomben, Handbook of X-ray Photoelectron Spectroscopy, Perkin-Elmer Corp, Eden Prairie, Minnesota, 1992.

[34] Y. Zhan, E. Holmström, R. Lizárraga, O. Eriksson, X. Liu, F. Li, E. Carlegrim, S. Stafström, M. Fahlman, Efficient spin injection through exchange coupling at organic semiconductor/ferromagnet heterojunctions, Adv. Mater. 22 (2010) 1626-1630.

[35] E. Otero, N. Kosugi, S.G. Urquhart, Strong double excitation and open-shell features in the near-edge x-ray absorption fine structure spectroscopy of ferrocene and ferrocenium compounds, J. Chem. Phys. 131 (2009) 114313:1- 8.

[36] B.M. Toner, S.C. Fakra, S.J. Manganini, C.M. Santelli, M.A. Marcus, J.W. Moffett, O. Rouxel, C.R. German, K.J. Edwards, Preservation of iron(II) by carbon-rich matrices in a hydrothermal plume, Nat. Geosci. 2 (2009) 197-201.

[37] M. Maric, M. Sohail, R. De Marco, A near edge X-ray absorption fine structure (NEXAFS) study of the response mechanism of the iron(III) chalcogenide glass membrane ion-selective electrode, Electrochem. Commun. 41 (2014) 27-30.

Table 1. Variation of the Cu-EN/Fe-EDTA buffer derived from alteration of the composition of EN relative to $CuSO_4$.

	Molar composition				
Solution	**$FeCl_3$**	**Na_2EDTA**	**$CuSO_4$**	**EN**	**NaCl**
Cu(1):EN(50)	10^{-4}	10^{-4}	10^{-3}	5×10^{-2}	0.6
Cu(1):EN(15)	10^{-4}	10^{-4}	10^{-3}	1.5×10^{-2}	0.6
Cu(1):EN(5)	10^{-4}	10^{-4}	10^{-3}	5×10^{-3}	0.6
Cu(1):EN(2)	10^{-4}	10^{-4}	10^{-3}	2×10^{-3}	0.6

Table 2. Equivalent circuit parameters for a RDE chalcogenide Fe(III) ISE in unbuffered 10^{-2} M $FeCl_3$ solution as a function of rotation speed (rpm).

Rotation Speed (rpm)	**R_{SOLN} (Ω)**	**Q_{CT} ($\Omega^{-1}s^n$)**	**n_{CT}**	**R_{CT} (kΩ)**	**log(rotation speed)**	**Log(1/R_{Ct})**
1000	66.2	2.60×10^{-5}	0.620	43.6	3.000	-4.640
2000	63.2	3.04×10^{-5}	0.758	35.8	3.301	-4.555
3000	54.4	3.25×10^{-5}	0.672	30.3	3.477	-4.482
4000	50.1	3.29×10^{-5}	0.634	24.8	3.602	-4.395
5000	54.8	3.50×10^{-5}	0.657	23.4	3.699	-4.367

Table 3. Equivalent circuit parameters for an iron(III) chalcogenide RDE treated in the seawater ligand mimetic system, an iron(III) chalcogenide RDE conditioned in natural seawater, a RDE chalcogenide Fe(III) ISE in an Fe-EDTA buffer, and a chalcogenide Fe(III) RDE conditioned in the ACS at 3000 rpm.

Sample	R_{SOLN} (Ω)	Q_{OSL} ($\Omega^{-1}s^n$)	n_{OSL}	R_{OSL} (kΩ)	Q_{MSL} ($\Omega^{-1}s^n$)	n_{MSL}	R_{MSL} (kΩ)	Q_{CT} ($\Omega^{-1}s^n$)	n_{CT}	R_{CT} (kΩ)
Seawater ligand mimic	21	4.2×10^{-5}	0.71	7.1	3.5×10^{-4}	0.63	26.4	8.3×10^{-3}	0.85	62.6
Seawater	19	6.0×10^{-5}	0.90	6.0	2.0×10^{-4}	0.70	30.0	5.0×10^{-4}	0.80	81.0
Fe-EDTA Buffer	20	9.0×10^{-5}	0.78	8.0	1.0×10^{-5}	0.70	60.0	6.5×10^{-4}	0.95	73.0
ACS	21	4.0×10^{-7}	0.88	5.3	3.6×10^{-5}	0.59	22.0	6.5×10^{-5}	0.30	82.0

Table 4. SR-XPS binding energies (eV) of the iron chalcogenide membrane exposed to a range of saline solutions for 1 day [ND = Not Detected, and the high binding energy shoulder on the Se(3d) level is included in parentheses in the row for $Se(3d_{5/2})$].

Level	**Polished**	**Brine**	**ACS**	**Seawater**
C(1s)	285.0, 286.6	285.0, 286.5	285.0, 286.5	285.0, 286.4, 288.7
$Fe(2p_{3/2})$	ND	ND	ND	ND
$Fe(2p_{1/2})$	ND	ND	ND	ND
Ge(3d)	30.9, 32.0	30.6, 32.2	30.4, 31.9	30.5, 32.1
$Se(3d_{3/2})$	54.4	54.7	54.4	54.7
$Se(3d_{5/2})$	53.9	53.9 (55.6)	53.9 (55.2)	53.8 (55.3)
$Sb(3d_{3/2})$	539.1	539.1	540.2, 539.0	538.9
$Sb(3d_{5/2})$	529.7	529.7	530.9, 529.6	529.5
O(1s)	533.0	533.0	532.9, 532.0	532.8
N(1s)	ND	ND	ND	400.0
$Cu(2p_{3/2})$	ND	ND	932.6	ND
$Cu(2p_{1/2})$	ND	ND	952.4	ND

Figure Captions

Figure 1: A schematic diagram of the CFA-ISE manifold.

Figure 2: (a) Levich equation plot of $\log(1/R_{CT})$ against log(rotation speed) for the iron(III) RDE in an unbuffered 10^{-2} M $FeCl_3$ solution; (b) equivalent circuit for the Fe(III) RDE ISE.

Figure 3: Nyquist plots generated for: (a) an iron chalcogenide RDE following exposure to the ACS system; (b) the Fe(III) RDE in seawater; and (c) the iron(III) chalcogenide RDE exposed to the Fe-EDTA buffer. Note that equivalent circuit fitted data derived using the equivalent circuit in Figure 2b have been overlaid as continuous lines on the raw EIS data that are depicted as graphical marks.

Figure 4: (a) CFA response and (b) calibration plot for a Fe(III) chalcogenide ISE at different $\log(aFe^{3+})$ values in a saline EDTA buffer for (i) -12.40, (ii) -14.66, (iii) -17.23, (iv) -18.65 and (v) -21.68.

Figure 5: (a) CFA responses and (b) calibration curve for a chalcogenide iron(III) ISE at different $\log(aFe^{3+})$ values in a saline Cu-EN/Fe-EDTA buffer system for (i) -20.70, (ii) -19.20, (iii) -16.30, (iv) -13.45 and (v) -10.66, along with (c) Bode phase plots of an iron(III) RDE subjected to seawater and various compositions of the Cu-EN/Fe-EDTA buffer system, as well as (d) Bode phase plots of the iron(III) sensor exposed to seawater and ACS.

Figure 6: (a) Iron(III) ISE CFA responses and (b) calibration plot in the seawater ligand mimetic calibration system proposed by Martizano and De Marco [18] and seawater. It should be noted the following $\log(aFe^{3+})$ values pertain to the calibration buffer for (i) -22.23, (ii) -18.84, (iii) -16.82, (iv) -14.36 and (v) -11.86, along with (c) iron(III) ISE CFA responses and (b) calibration plot in the ACS and seawater at the following $\log(aFe^{3+})$ values in the calibration system for (i) -22.08; (ii) -17.17, (iii) -15.04, (iv) -12.77 and (v) -10.34.

Figure 7. (a) N(1s) spectra following exposure of the chalcogenide membrane to natural seawater, and (b) normalized Fe(2p) NEXAFS spectra of the Fe(III) ISE chalcogenide membrane conditioned in different calibration media.

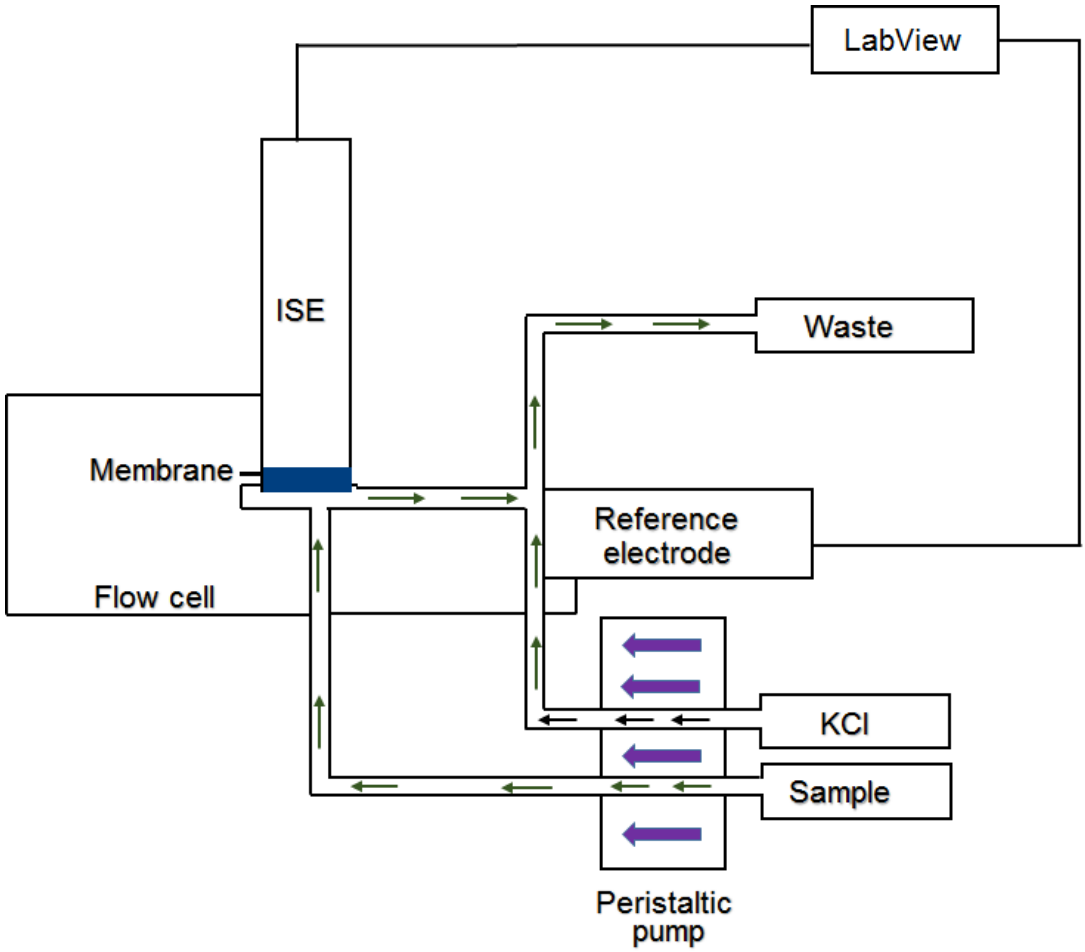

Figure 1

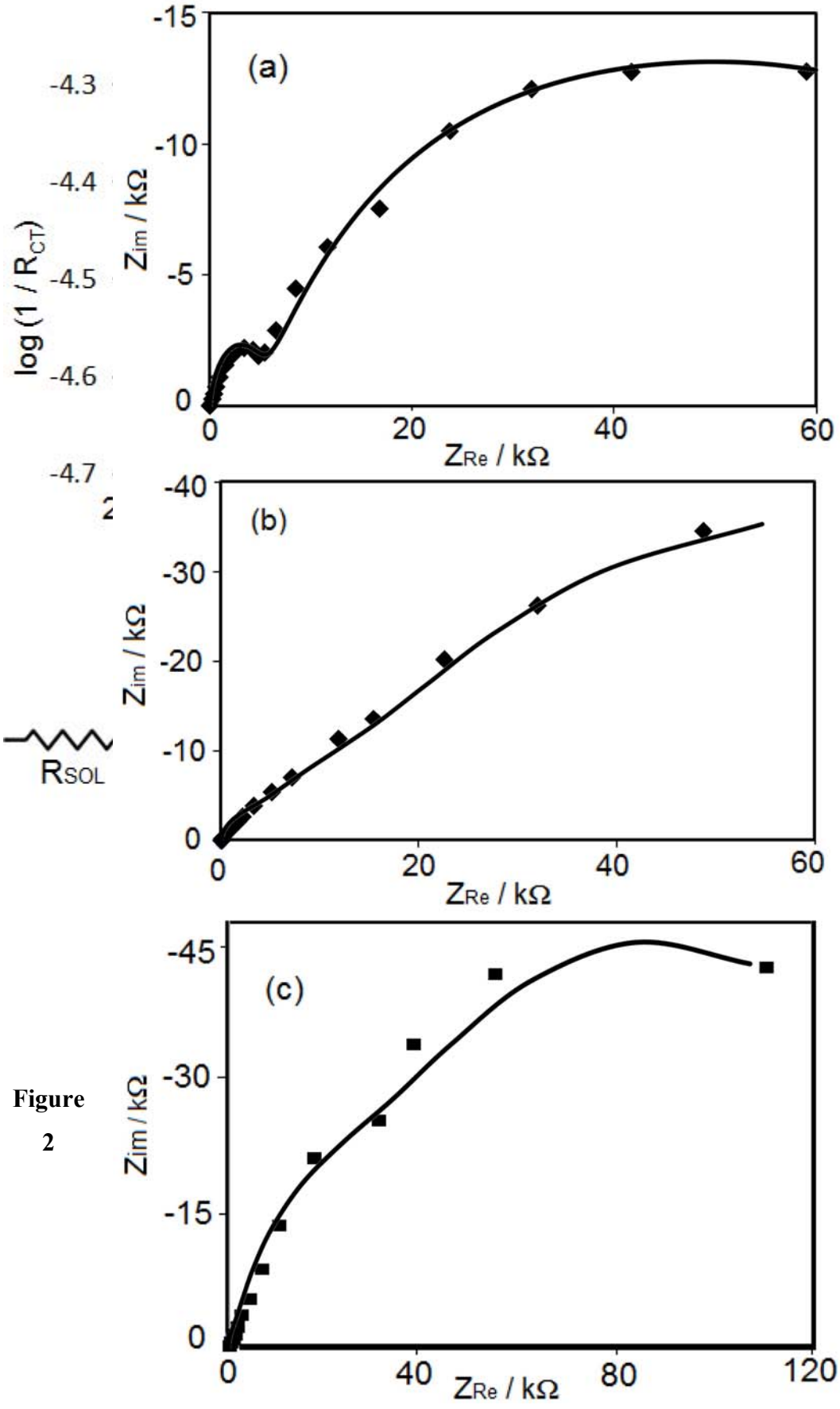

Figure 2

Figure 3

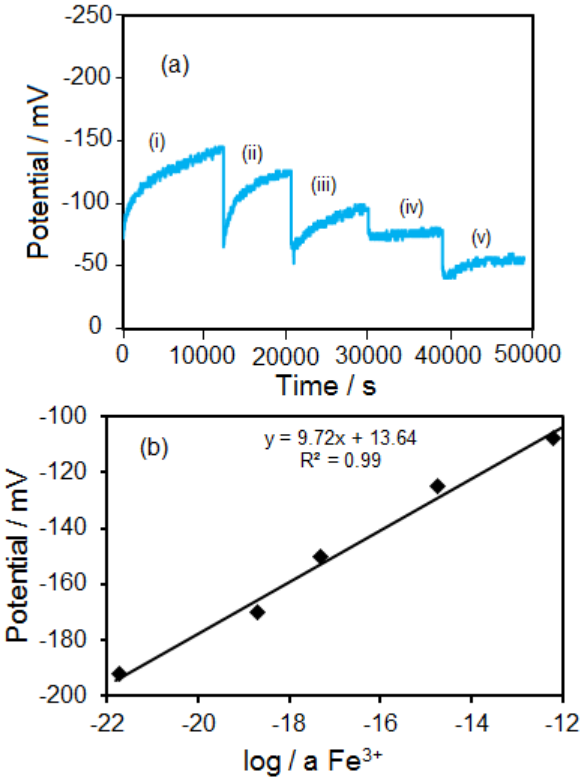

Figure 4

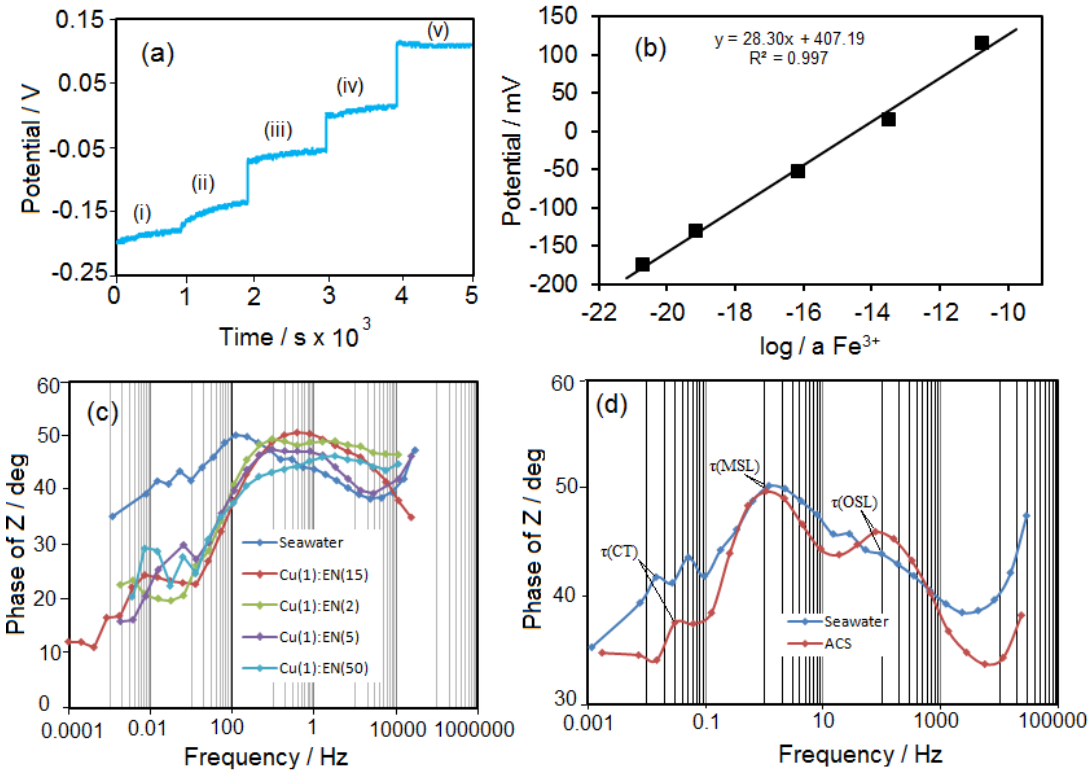

Figure 5

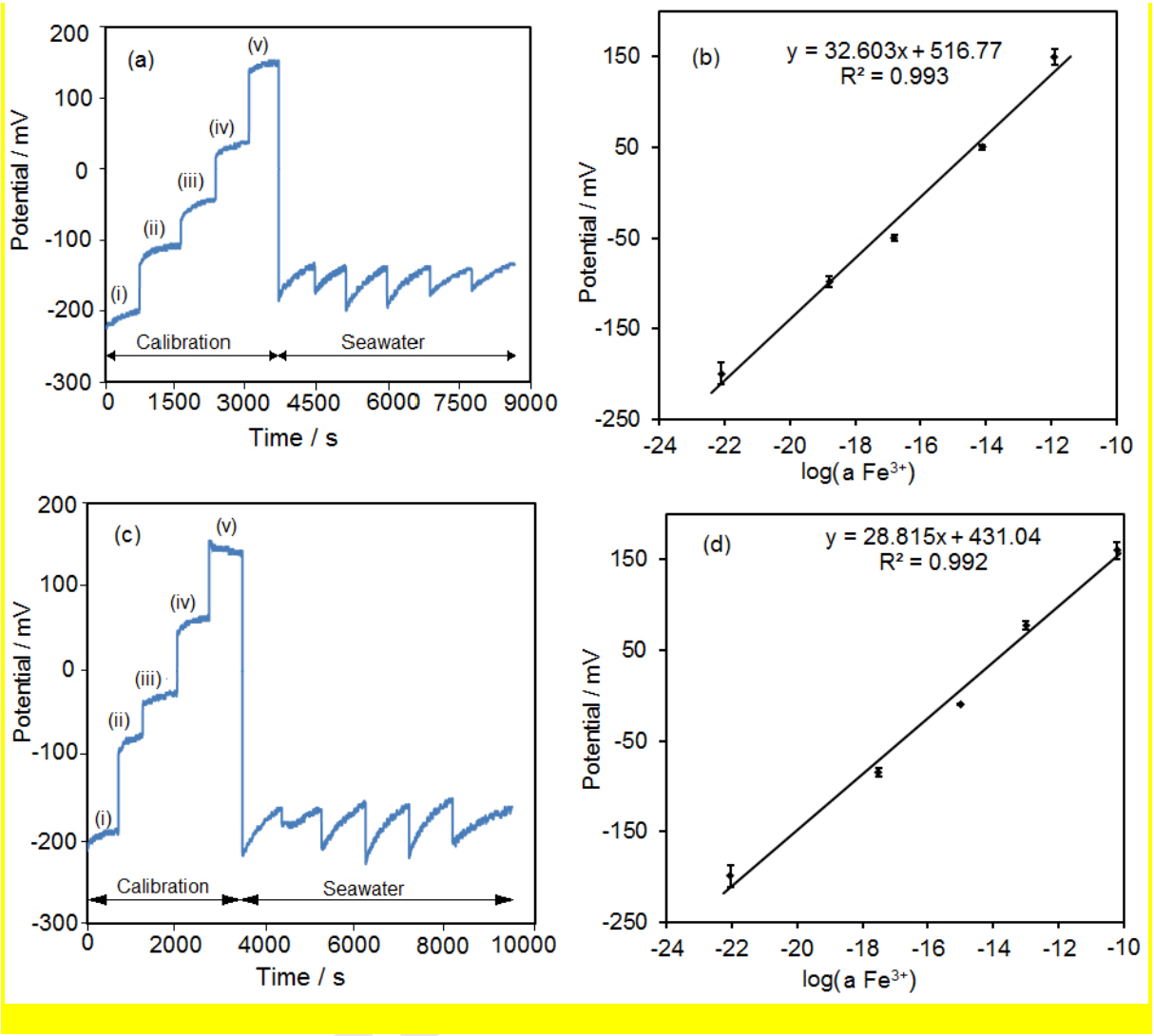

Figure 6

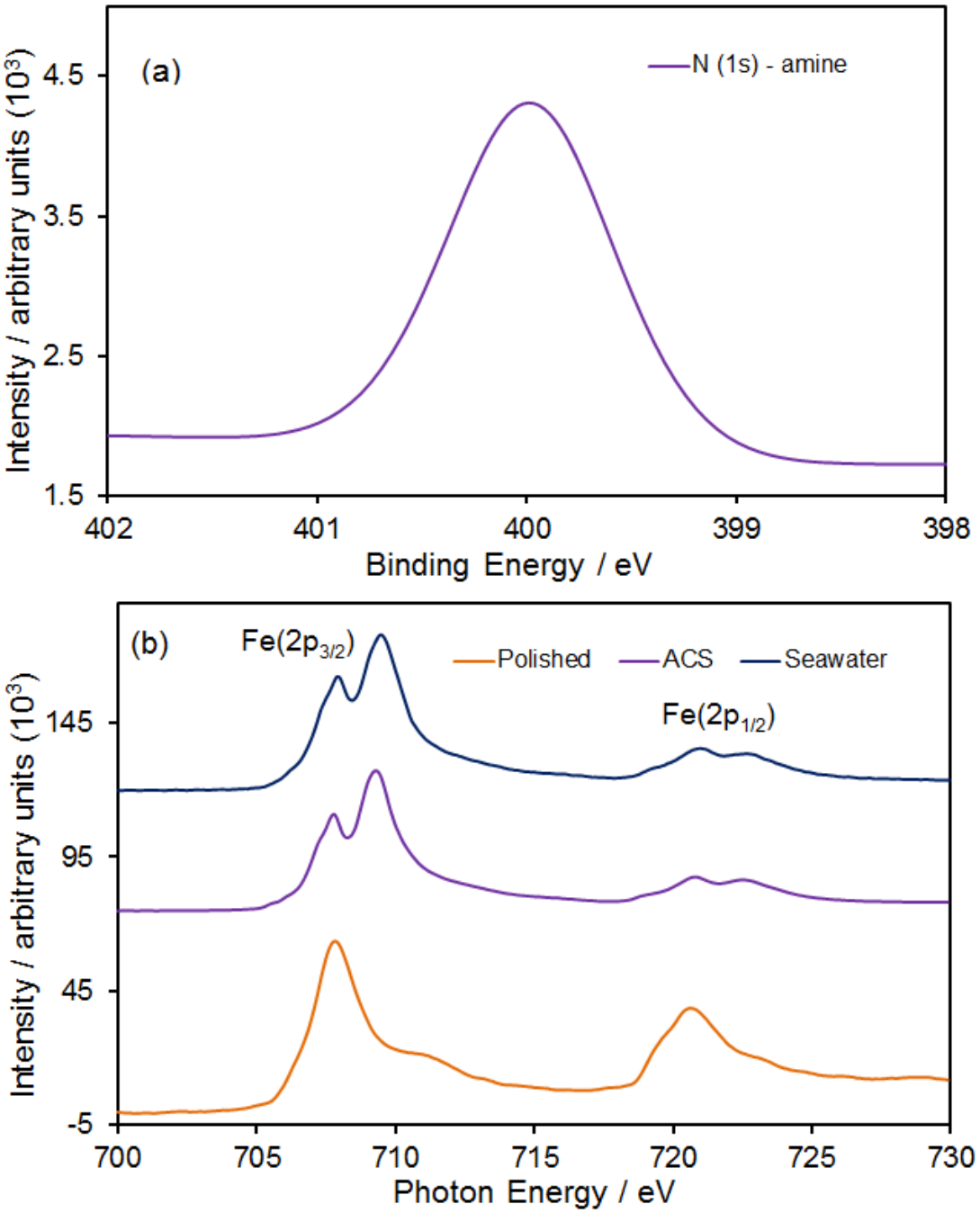

Figure 7

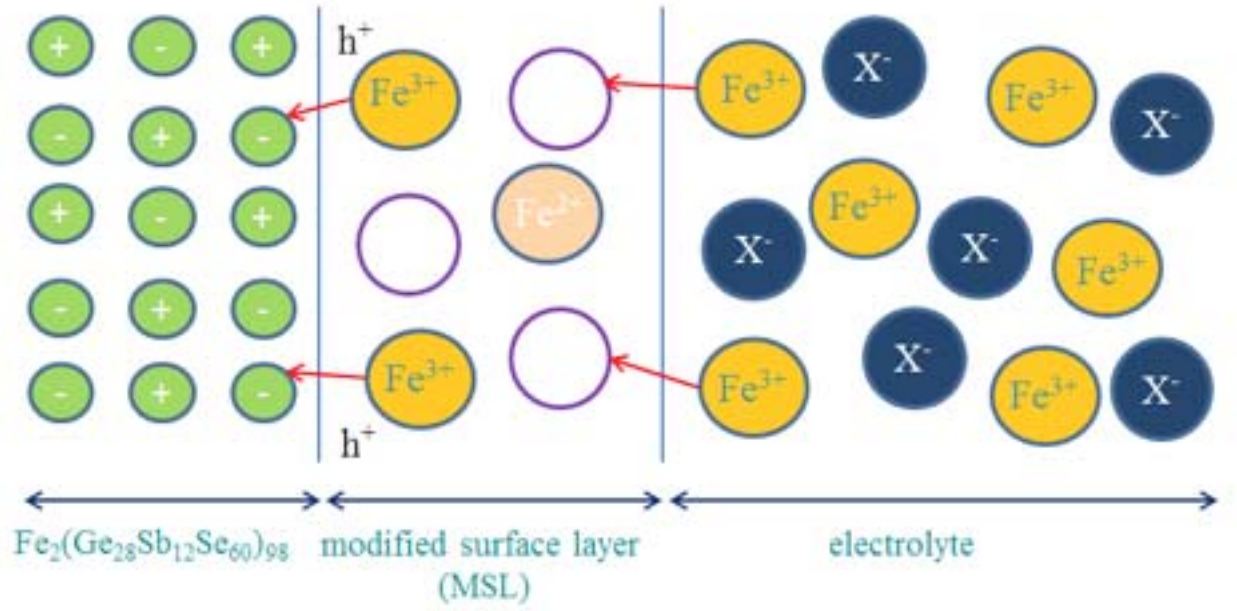

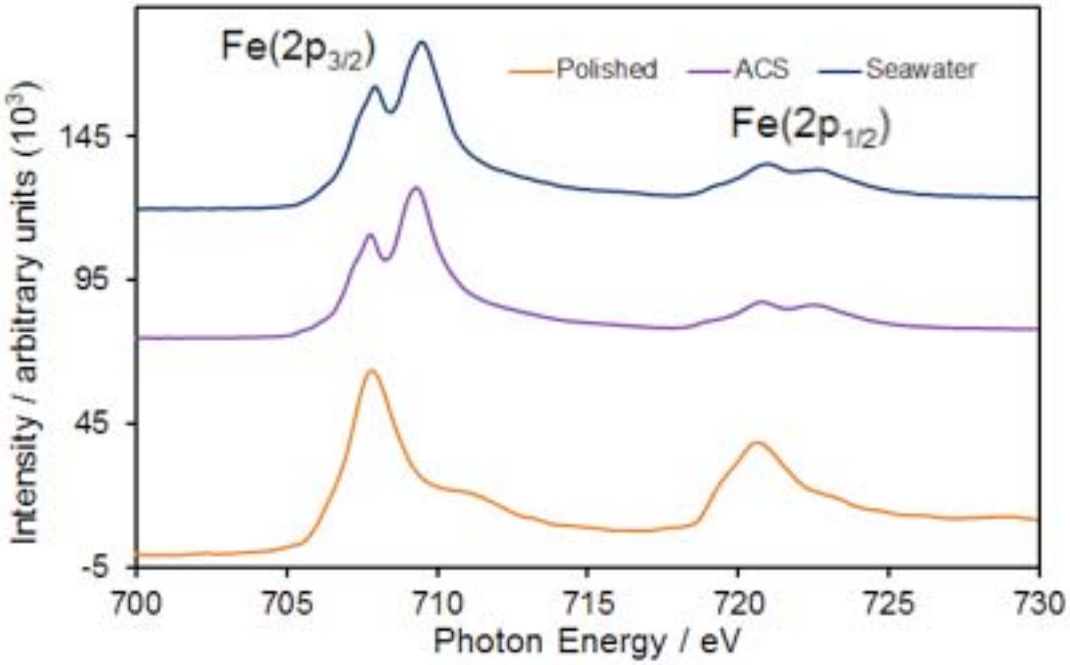

Highlights

- Improved calibration system for the iron(III) electroanalysis of seawater.
- Alternative calibration system for the chalcogenide based iron ion selective electrode.
- Evidence of surface reactions using SR-XPS and NEXAFS.
- Improved analysis of iron(III) in seawater.

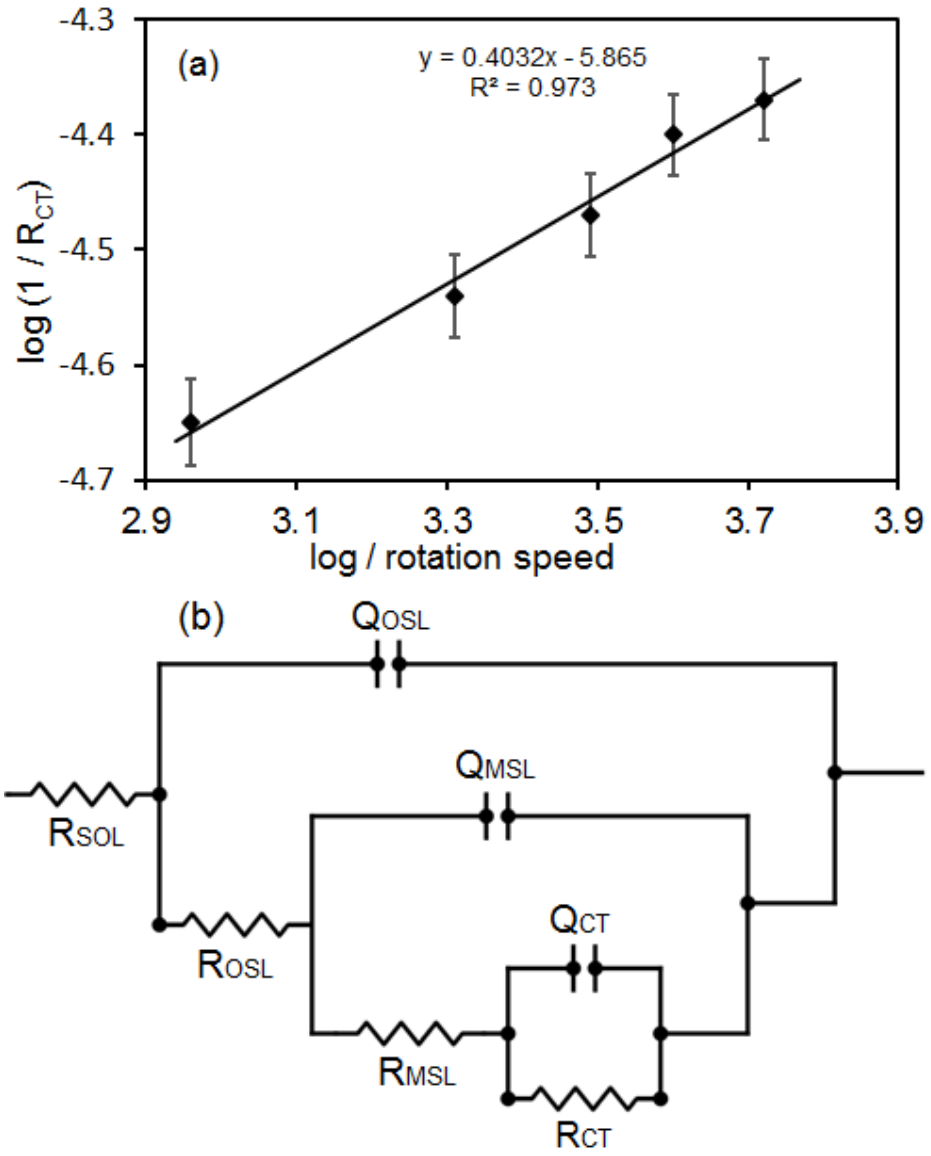

Figure 2